X-Ray Synchrotron Study of Liquid-Vapor Interfaces at Short Length Scales: Effect of Long-Range Forces and Bending Energies

S. Mora and J. Daillant
LURE, Centre Universitaire Paris-sud, bâtiment 209D, BP34, F-91898 Orsay cedex, France
Service de Physique de l'Etat Condensé, Orme des Merisiers, CEA Saclay, F-91191 Gif-sur-Yvette Cedex, France

K. Mecke
Max-Planck Institut für Metallforschung, Heisenbergstrasse 1, D-70569 Stuttgart, Germany

D. Luzet and A. Braslau
Service de Physique de l'Etat Condensé, Orme des Merisiers, CEA Saclay, F-91191 Gif-sur-Yvette Cedex, France

M. Alba
Laboratoire Léon Brillouin, CEA Saclay, F-91191 Gif-sur-Yvette Cedex, France

B. Struth
European Synchrotron Radiation Facility, B.P. 220, F-38043 Grenoble Cedex, France
(Received 21 October 2002; published 27 May 2003)

We have investigated the small-scale structure of the liquid-vapor interface using synchrotron x-ray scattering for liquids with different molecular structures and interactions. The effective momentum-dependent surface energy first decreases from its macroscopic value due to the effect of long-range forces, and then increases with increasing wave vector. The results are analyzed using a recent density functional theory. The large wave-vector increase is attributed to a bending energy for which local and nonlocal contributions are equally important.

DOI: 10.1103/PhysRevLett.90.216101 PACS numbers: 68.03.Cd, 61.10.Kw

Liquid interfaces are of fundamental importance in many areas of science and technology and have been the subject of continuous attention since van der Waals [1]. It is, however, only in recent years that a continuous effort on theory [2], experimental methods [3], and numerical simulations [4,5] has given us a more complete picture of their microscopic structure.

In the approach initiated by van der Waals [1,6], the interface was described as a region of smooth transition (intrinsic profile) from the density of the liquid to that of the gas over approximately the bulk correlation length ξ. Conversely, the 1965 capillary-wave model of Buff, Lovett, and Stillinger [7] describes a wandering, steplike interface whose structure is determined by the height correlation spectrum $\langle z(q_\parallel)z(-q_\parallel)\rangle \propto k_BT/\gamma q_\parallel^2$, where γ is the surface tension and $2\pi/q_\parallel$ is the wavelength of the capillary excitation, in good agreement with experiments [8,9]. This description is necessarily expected to fail at small length scales, at least for $2\pi/q \approx \xi$ [10]. Since the interfacial structure is determined by the surface energy associated with the deformation modes, the problem of the small-scale structure can be addressed by considering corrections to the surface energy through an effective Hamiltonian or wave-vector-dependent surface energy $\gamma(q_\parallel)$. Following Helfrich [11], the surface free energy can be expanded in powers of the mean curvature H and of the Gaussian curvature. Fourier transforming and applying the theorem of equipartition of energy, one obtains

$$\gamma(q_\parallel) = \gamma + \kappa q_\parallel^2, \tag{1}$$

where $\gamma \equiv \gamma(q_\parallel = 0)$ is the macroscopic surface tension and κ is the bending rigidity constant. In a previous study [3], we found a large reduction in the surface energy of water with increasing wave vectors which was in strong contradiction with an expected positive bending rigidity. Our results could, however, be successfully interpreted using a density functional theory [2] which shows that the analytical expansion Eq. (1) cannot be performed in the presence of long-range forces and predicts that the surface tension should reach its macroscopic value from below in the limit $q_\parallel \to 0$. In this Letter, using an improved experimental setup and analysis procedure, we are able to give a more complete description (including the large q limit) of liquid interfaces for different liquids (Fig. 1, Table I): octamethylcyclotetrasiloxane (OMCTS) and carbon tetrachloride (CCl_4) considered as model Lennard-Jones liquids, a branched alkane, squalane, as well as water and ethylene glycol whose properties are largely determined by hydrogen bonds.

Within the distorted-wave Born approximation [14–16], which is currently the most accurate theory for the analysis of x-ray surface scattering experiments, the scattering cross section (power radiated per unit solid angle in the scattering direction per unit incident flux) can be approximated by

$$\left(\frac{d\sigma}{d\Omega}\right) \approx \mathcal{A}\,\frac{k_0^4\theta_c^4}{16\pi^2}\cos^2\psi |t^{\rm in}|^2 |t^{\rm sc}|^2 \left[\frac{k_B T}{\gamma(q_\parallel) q_\parallel^2}\left(\frac{q_\parallel e^{-\Gamma_e}}{q_{\rm max}}\right)^{\eta} \frac{\Gamma(1-\eta/2)}{\eta/2\Gamma(\eta/2)} + \frac{k_B T \kappa_T}{2\,{\rm Im}(q_z^{\rm t})}\right], \quad (2)$$

where Γ is Euler's function, Γ_e is Euler's constant, and $\eta = k_B T |q_z^{\rm t}|^2/(2\pi\gamma(q_\parallel))$. The first contribution within the square brackets, due to the surface fluctuations [9,17,18] (capillary waves), reduces to $k_B T/\gamma(q_\parallel) q_\parallel^2$ for small η. The second one is due to propagating and nonpropagating density fluctuations just below the surface (κ_T is the isothermal compressibility). The imaginary part of the vertical component of the transmitted wave-vector transfer in the liquid ${\rm Im}(q_z^{\rm t})$ fixes the effective penetration length of the x-ray radiation. The largest wave vector in the capillary-wave spectrum $q_{\rm max}$ is on the order of an inverse molecular diameter. $\mathcal{A}$ is the illuminated area on the surface, and $t^{\rm in}$ and $t^{\rm sc}$ are the Fresnel transmission coefficients for the incident and scattering angles, respectively. Comparing calculated and experimental intensity on an absolute scale is an important issue. For this, the resolution function has been carefully determined following [15] and folded with the scattering cross section. We have also verified that an excellent agreement was obtained without any fit for small enough $q_\parallel$ values for which the macroscopic surface tension can be used in Eq. (2).

The experiments reported here used a 8.00 keV x-ray beam (wavelength $\lambda = 0.155$ nm) at the Troika II beam line of the European Synchrotron Radiation Facility; see Fig. 2. We used ultrapure deionized water from a Milli-Q 185+ Millipore system; CCl_4 (Sigma, 99.9% purity), squalane (Fluka, 99%), OMCTS (Fluka, 99%), and ethylene glycol (Aldrich, 99.5%) were used without further purification. The monochromatic incident beam was first extracted from the polychromatic beam of the undulator source using a two-crystal diamond (111) monochromator. Higher harmonics were eliminated using two platinum coated glass mirrors, also used to set the grazing angle of incidence $\theta_{\rm in}$ on the liquids which were contained in a Teflon trough mounted on an active antivibration system. $\theta_{\rm in}$ was fixed to either 2.00 or 3.20 mrad. Depending on whether $\theta_{\rm in}$ is below or above the critical angle for total external reflection θ_c (which occurs for x rays since the refractive index of matter is less than 1), the effective penetration length $1/2\,{\rm Im}(q_z^{\rm t})$ varies from a few nm (evanescent wave) to more than 10 μm (Table I), allowing the control of the relative weight of the surface and bulk terms. The resolution was set by different slits (Fig. 2), giving an in-plane resolution $\Delta q_\parallel = 2.7 \times 10^7$ m^{-1}, and the scattered signal was collected using a vertically mounted position sensitive detector (PSD). Extreme care was taken to minimize the background, which is essential in order to measure the very small high $q_\parallel$ surface signal (less than 10^{-11} of the incident intensity). The incident and scattered beams traveled through vacuum paths, and the measurements were performed under a vapor saturated helium atmosphere. The residual background was recorded and subtracted [19] by lowering the trough and scanning around the direct beam (transposed by twice the incident angle). Since the experiment is performed under *total* external reflection, though the reflected beam and the transmitted beam (when the sample is lowered) follow different paths,

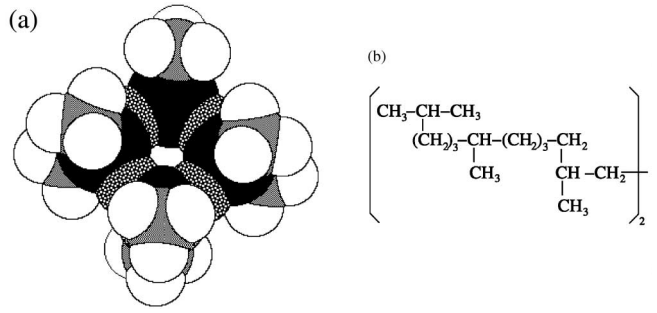

FIG. 1. (a) OMCTS ($[(CH_3)_2SiO]_4$; black = Si, black and white = O, grey = C, white = H) is inert and of low polarity ($\mu \simeq 0.42$ D). The molecular diameter is $\simeq 0.75$–0.85 nm [12]. (b) Squalane ($C_{30}H_{62}$) with 6 methyl groups symmetrically placed along a 24 carbon backbone is a soft sphere with gyration radius $\simeq 0.7$ nm [13].

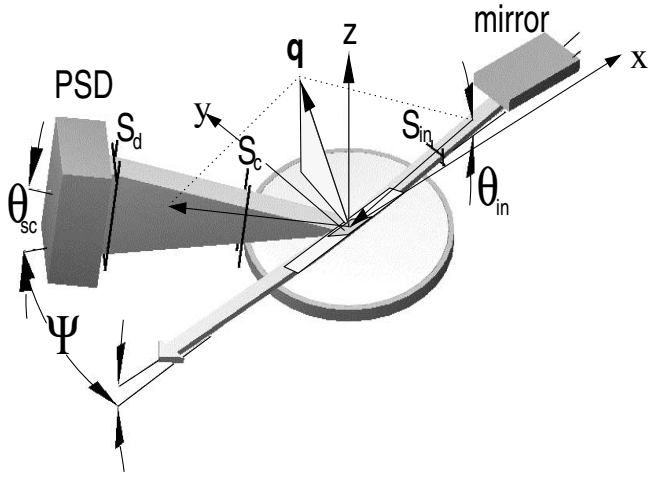

FIG. 2. Schematic view of the experiment. The Teflon trough (inner diameter = 330 mm) is mounted on an active antivibration system. The size of the incident beam is fixed by a 275 μm × 250 μm ($H \times V$) slit. The horizontal resolution of the experiment is fixed by the slits S_c, 300 μm wide, and S_d, 545 μm wide, placed at 254 and 882 mm from the sample, respectively, as well as by the illuminated area seen by the detector (dark grey paralleogram). $\mathbf{q}$ is the wave-vector transfer whose in-plane component is $\mathbf{q}_\parallel$.

TABLE I. Room temperature characteristics of the liquids used in this study. ρ is the density, κ_T is the isothermal compressibility determined by fitting the data to Eq. (2), γ is the macroscopic surface tension, θ^c is the critical angle for total external reflection at 8.00 keV, $1/(2\,\mathrm{Im}q_z^t)$ is the effective penetration length for $\theta^{\mathrm{in}} = 2.0$ mrad, $2\pi/q$ is the distance determined from the position of the liquid peak in the present study (not shown here), d is the intermolecular distance by other methods, and ϵ is the depth of the Lennard-Jones potential. ξ_0^{lit} and r_0^{lit} are deduced from literature, whereas ξ^{fit} and r_0^{fit} are from fits of the experimental $\gamma(q_\parallel)$.

	ρ (10^{27} m^{-3})	κ_T (10^{-10} m^2 N^{-1})	γ (mN/m)	θ^c (mrad)	$1/(2\,\mathrm{Im}q_z^t)$ (nm)	$2\pi/q$ (nm)	d (nm)	ϵ 10^{-21} J	ξ_0^{lit} (nm)	r_0^{lit} (nm)	ξ^{fit} (nm)	r_0^{fit} (nm)
OMCTS	1.94	$\simeq 70$	18	2.60	7.2	0.84	0.79 [12]	4.74 [12]	1.5	0.42	1.75 ± 0.4	0.43 ± 0.09
CCl_4	6.24	8.9	30	3.01	5.3	⋯	0.62 [21]	5.20 [21]	1.1	0.52	$1.3(<7)$	1.4 ± 1
Squalane	1.15	$\simeq 45$	28	2.45	8.5	0.50	⋯	⋯	⋯	⋯	2.0 ± 0.6	0.88 ± 0.15
Water	33.4	4.5	73	2.70	6.6	0.28	0.25	⋯	∼0.3	⋯	0.66 ± 0.6	0.70 ± 0.08
Ethylene glycol	1.08	3.7	46	2.60	6.5	0.42	⋯	⋯	⋯	⋯	$0.55(<2)$	0.83 ± 0.02

both have exactly the same length and intensity. Hence the background is the same.

The wave-vector dependent surface energy can be obtained in two ways: The first possibility consists of dividing the intensity due to capillary waves [first term between square brackets in Eq. (2)] calculated using the macroscopic surface tension γ, by the measured intensity after subtraction of the bulk contribution, leading to $\gamma(q_\parallel)/\gamma$. The other possibility is to directly extract $\gamma(q_\parallel)$ from a fit of each curve recorded on the PSD for a given $q_\parallel$ (Fig. 3). Both methods give the same result (Fig. 4), which is a check of the measurement accuracy. In order to get insight into the physics of the liquid-vapor interface, we analyzed our results using the theory of Ref. [2]. This density functional theory is constructed by describing the liquid using the Carnahan-Starling equation of state, and long-range interactions with a potential $w(r) = -w_0 r_0^6/(r^2 + r_0^2)^3$. An effective interfacial Hamiltonian is constructed as the difference between the grand potential minimized with the constraint of a given density on a given deformed surface, and that for the flat interface, leading to a momentum-dependent surface tension:

$$\gamma(q_\parallel) = 4\frac{\tilde{h}(0) - \tilde{h}(q_\parallel)}{q_\parallel^2} + 2[\tilde{\kappa}^H(q_\parallel) - \tilde{\kappa}^H(0)] + \kappa q_\parallel^2 - \tilde{\kappa}^{HH}(q_\parallel) q_\parallel^2 + \mathcal{O}(q_\parallel^4). \quad (3)$$

The density distribution at the fluctuating interface is different from the flat intrinsic density profile because there is a displacement of the average interface position (capillary waves), and also because curvature induces density changes in the intrinsic profile. The first term in Eq. (3) gives the contribution of long-range forces due to interface displacement, neglecting the distortion in the intrinsic profile, and the other terms are bending terms, either local [$\kappa q_\parallel^2$ like in Eq. (1)] or nonlocal (due to long-range interactions). The $\tilde{\kappa}^{HH}(q_\parallel) q_\parallel^2$ term describes the long-range interactions between distorted regions of the intrinsic profile, whereas the $\tilde{\kappa}^H$ terms describe the coupling between distortions in the intrinsic profile and interface displacement. For simplicity we use in the following the simpler "product" approximation [2] which amounts to neglecting density changes normal to the interface in the integration of the effective Hamiltonian. It is therefore valid if $r_0 \ll \xi$, but remains accurate to $\approx 10\%$ even for $\xi \approx r_0$ [2]. The approximation does not, however, correctly describe the behavior $\sim q^2 \ln q$ for $q \to 0$. Within this approximation, $\tilde{h}(q_\parallel) = -\gamma(1 + q_\parallel r_0) e^{-q_\parallel r_0}/2r_0^2$, $\tilde{\kappa}^H(q_\parallel) = -1/2 C_H (\xi/r_0)^2 \gamma(1 + q_\parallel r_0) e^{-q_\parallel r_0}$, $\tilde{\kappa}^{HH}(q_\parallel) = 0.74 C_H^2 \xi^4/r_0^2 \gamma(1 + q_\parallel r_0) e^{-q_\parallel r_0}$, and $\kappa = 0.74 C_H^2 \xi^2 (1/2 + \xi^2/r_0^2)\gamma$. C_H is the "susceptibility" of the density profile to curvature (see [2]), with the curvature corrections to the profile being proportional to C_H. Landau theory gives $C_H = 0.25$ which we use in the following. Using Eq. (3) with this value yields a good description of the experimental data (Fig. 4). Good fits could be obtained only for $0 \lesssim C_H \lesssim 0.4$.

ξ and r_0 values that best fit $\gamma(q_\parallel)$ are given in Table I. It is interesting to compare these values to ξ and when possible r_0 values determined by other methods. Using the isothermal compressibility κ_T (Table I) and w_0 and r_0 deduced from literature by adjusting the long-range tail of $w(r)$ to known Lennard-Jones potentials [20,21], ξ can

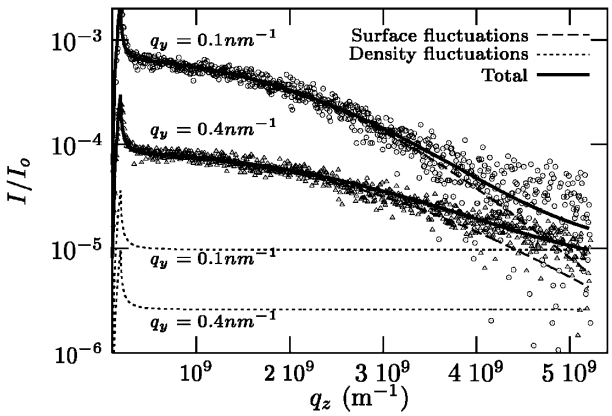

FIG. 3. Signal recorded on the PSD for in-plane wave-vector transfers $q_y = 10^8$ m^{-1} (○) and $q_y = 4 \times 10^8$ m^{-1} (△) for OMCTS. The solid line is the best fit [via $\gamma(q_\parallel)$, κ_T, and $q_{\max}$] to Eq. (2); long and short dashed lines are, respectively, surface and bulk contributions as explained in the text.

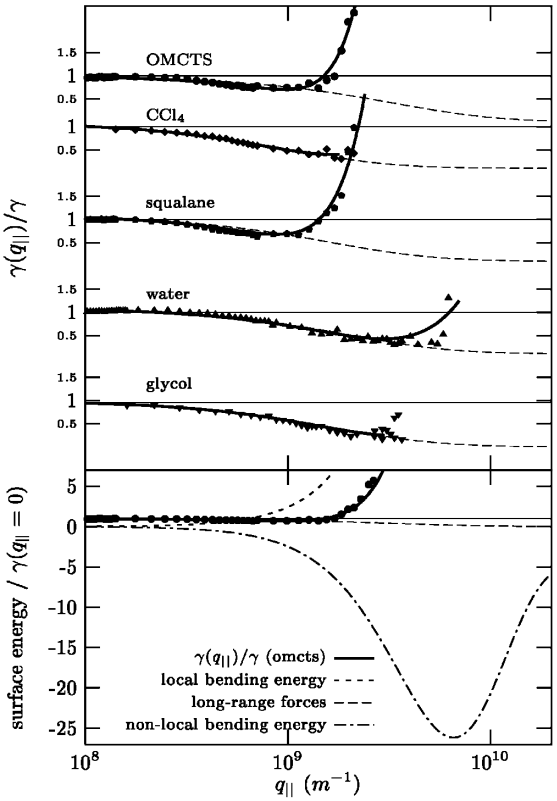

FIG. 4. $\gamma(q_\parallel)/\gamma$ for OMCTS, carbon tetrachloride, squalane, water, and glycol. Lines are the best fits using Eq. (3). Dashed lines give the long-range forces contribution (excluding nonlocal bending energy). Bottom: Contribution of long-range forces, local bending energy, and nonlocal bending energy to the momentum dependent surface tension for OMCTS.

be obtained as $\xi^2 = 3/4\pi^2\rho^2\kappa_T w_0 r_0^5$ [2]. The agreement between the fit and literature values of ξ and r_0 is excellent for the Lennard-Jones liquids (Table I) CCl_4 (for which the experimental incertitude is high due, in particular, to a large vapor pressure), and above all for OMCTS. Although internal degrees of freedom of a branched alkane [22] like squalane are ignored by the theory, the long-range part of the potential is expected to behave as r^{-6}, and the experimental data are well described by the theory. Molecular interactions involving hydrogen bonds (water and ethylene glycol) do not follow a Lennard-Jones potential [23] if the bonding of two specific molecules is considered, but the orientational smearing out of the microscopic details due to thermal averaging make the differences qualitatively unimportant and the agreement is again quite good (Table I).

The initial decrease in surface energy from γ evidenced for water in Ref. [3] has now been obtained for different liquids with different molecular structure and interactions, adding evidence to the attribution of this effect to the omnipresent dispersion forces. At larger wave vectors, we find an increase in surface energy, which is well described by theory and, at least for OMCTS and squalane allows a precise discussion of bending energies. The most important point is that the local bending energy, $\kappa q_\parallel^2$, although formally determining the $q_\parallel \to \infty$ behavior, is strongly reduced by the nonlocal contributions for practical $q_\parallel$ values smaller than $2\pi/d$ (Table I). This is illustrated for OMCTS in Fig. 4, where the different contributions are separated. Most striking is that the total bending energy results from a partial compensation of the local contribution by the nonlocal contribution, both of them being much larger than their sum. The usual, local term, is not at all dominant. Also important is that an asymptotic q^2 behavior is never reached for realistic $q_\parallel$ values.

[1] J. D. van der Waals, Verh. K. Akad. Wet. Amsterdam (Sect. 1) **1**, 8 (1893).
[2] K. R. Mecke and S. Dietrich, Phys. Rev. E **59**, 6766–6784 (1999).
[3] C. Fradin *et al.*, Nature (London) **403**, 871–874 (2000).
[4] J. Stecki, J. Chem. Phys. **109**, 5002–5007 (1998).
[5] A. E. van Giessen and E. M. Blokhuis, J. Chem. Phys. **116**, 302–310 (2002).
[6] J.W. Cahn and J. E. Hilliard, J. Chem. Phys. **28**, 258–267 (1958).
[7] F. P. Buff, R. A. Lovett, and R. H. Stillinger, Phys. Rev. Lett. **15**, 621–623 (1965).
[8] R. Loudon, in *Modern Problems in Condensed Matter Sciences*, edited by V. M. Agranovich and R. Loudon (North-Holland, Amsterdam, 1984), Vol. 9, pp. 589–638.
[9] M. K. Sanyal *et al.*, Phys. Rev. Lett. **66**, 628–631 (1991).
[10] J.V. Sengers and J. M. J. van Leeuwen, Phys. Rev. A **39**, 6346–6355 (1989).
[11] W. Helfrich, Z. Naturforsch. **28c**, 693–703 (1973).
[12] R. G. Horn and J. Israelachvili, J. Chem. Phys. **75**, 1400 (1981).
[13] M. Mondello and G. S. Grest, J. Chem. Phys. **103**, 7156 (1995).
[14] S. K. Sinha, E. B. Sirota, and S. Garoff, Phys. Rev. B **38**, 2297–2311 (1988).
[15] J. Daillant and O. Bélorgey, J. Chem. Phys. **97**, 5837–5843 (1992).
[16] S. Dietrich and A. Haase, Phys. Rep. **260**, 1–138 (1995).
[17] M. Fukuto *et al.*, Phys. Rev. Lett. **81**, 3455–3458 (1998).
[18] H. Tostmann *et al.*, Phys. Rev. B **59**, 783–791 (1999).
[19] C. Gourier *et al.*, Phys. Rev. Lett. **78**, 3157–3160 (1997).
[20] J. E Curry, J. Chem. Phys. **113**, 2400–2406 (2000).
[21] P.W. Atkins, *Physical Chemistry* (Oxford University Press, Oxford, 1998), 7th ed.
[22] J. I. Siepmann, S. Karaborni, and B. Smit, Nature (London) **365**, 330–332 (1993).
[23] M.W. Mahoney and W. L. Jorgensen, J. Chem. Phys. **112**, 8910–8922 (2000).